Bubbling up in a Lab-on-a-Chip: A gravity-driven approach to the formation of polyelectrolyte multilayer capsules and foams

Stéphane Pivard, Aurélie Hourlier-Fargette, Guillaume Cotte-Carluer, Duzhi Chen, Antoine Egele, Christophe Lambour, Francois Schosseler, Wiebke Drenckhan-Andreatta

Colloids and Surfaces A: Physicochemical and Engineering Aspects 700 (2024) 134608

Contents lists available at ScienceDirect

Colloids and Surfaces A: Physicochemical and Engineering Aspects

journal homepage: www.elsevier.com/locate/colsurfa

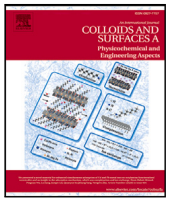

Bubbling up in a Lab-on-a-Chip: A gravity-driven approach to the formation of polyelectrolyte multilayer capsules and foams

S. Pivard, A. Hourlier-Fargette, G. Cotte-Carluer, D. Chen, A. Egele, C. Lambour, F. Schosseler, W. Drenckhan-Andreatta *

Institut Charles Sadron, CNRS UPR22 - Strasbourg University, 23 rue du Loess, Strasbourg, 67034, France

GRAPHICAL ABSTRACT

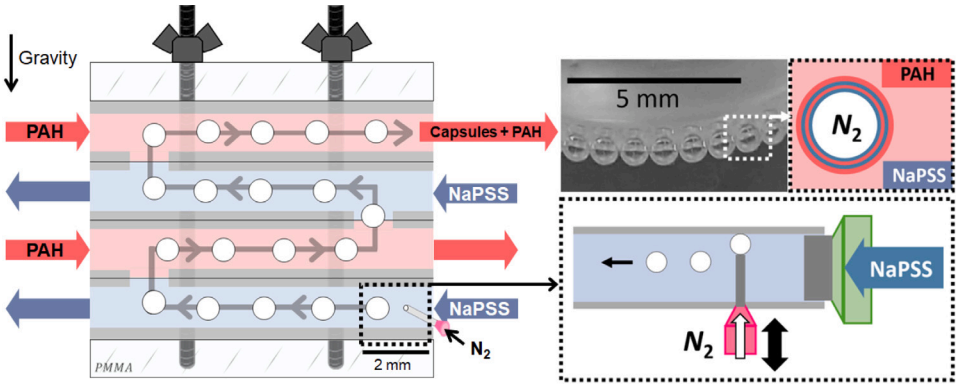

HIGHLIGHTS

- New millifluidic method exploits mobile dispensing tip to tune bubbling.
- Bubble size and spacing are independently controlled.
- Novel method moves bubbles between strata of a millifluidic chip by gravity.
- Flow of bubbles through alternating strata creates multilayer PSS/PAH capsules.
- Obtained capsules have lifetimes of the order of several months.

ARTICLE INFO

Keywords:
Millifluidics
Coated air bubbles with tunable size and enhanced longevity
Polyelectrolyte multilayers
Functional coating
Polymer capsules

ABSTRACT

The generation of multi-functional capsules often requires the sequential deposition of different components on the surface of bubbles or drops. Batch-based methods lack fine control over the capsule sizes, including risk of fusion, and cannot ensure identical environments for each capsule. To overcome these issues, different micro/milli-fluidic methods have been developed in the past. However, a major challenge remains in combining an explicit and flexible control over the capsule generation and their residence time in the different solutions within the same device. Using for the first time the example of bubbles covered by layers of oppositely charged polyelectrolytes (PSS/PAH), we introduce an original millifluidic Lab-on-a-Chip device with two novel functions: (1) Size and separation of the bubbles are tuned at constant flow conditions via gas injection through a movible, circular dispense tip into the cross-flow of a rectangular channel. We provide a detailed exploration of the bubbling parameters together with physical justification of the observations. (2) The device exploits

* Corresponding author.
E-mail address: drenckhan@unistra.fr (W. Drenckhan-Andreatta).

https://doi.org/10.1016/j.colsurfa.2024.134608
Received 17 April 2024; Received in revised form 10 June 2024; Accepted 24 June 2024
Available online 3 July 2024

gravity to make the generated bubbles rise between horizontally stacked millifluidic chips containing each the controlled flow of a specific polyelectrolyte solution. In analogy with electric circuits, we show how the flow resistance of each chip can be adapted such that bubbles move smoothly between them while avoiding undesired mixing of the solutions. We show first examples of obtained multilayer capsules and discuss their peculiar features, in particular, their outstanding stability with respect to coalescence and dissolution. While our methods use polyelectrolyte assembly on bubbles, they can be readily transferred to other types of solutions or even to drops and particles.

1. Introduction

The use of multifunctional liquid or gaseous capsules is entering an increasing number of domains (medicine, cosmetics, food, agriculture, etc.) due to the possibility of combining a controlled capsule size with purpose-designed mechanical properties, fine-tuned release kinetics and/or with specific surface functionalities [1–5]. Batch-based methods, used in the past to create these capsules, are increasingly replaced by micro- or millifluidic approaches, which ensure an explicit control over the size and formulation of each capsule [6,7]. While this works well for simple capsule architectures, it remains a challenge for more complex constructions, requiring the combination of different washing, soaking or deposition steps.

Here we shall focus on the example of capsules coated with polyelectrolyte (PE) multilayers [8–18]. These are generated by passing the capsule core in an alternating manner through solutions of polyelectrolytes with opposite charges, separated by a washing step. The capsule cores may be solid, liquid or gaseous. Often, the solid or liquid core is removed in a final step to obtain a hollow capsule [8,10,11,13,17]. While, to the best of our knowledge, no study has been published to generate directly gaseous PE multilayer capsules, different authors present microfluidic approaches to the coating of particles or droplets [19–26].

For example, Madisetti et al. [19] perform PE multilayer deposition on poly(dimethyldiallyl ammonium chloride)-coated poly(methacrylate) core droplets, which are subsequently coated with sodium poly(styrene sulfonate) (NaPSS) using a cascade droplet-generating device to adsorb NaPSS after rinsing. Trégouët et al. [21,22] combine the microfluidic generation of oil drops with a channel geometry containing small pillars which allow the liquid to pass, but not the drops. This enables to separate the flow of the drops from that of the liquid in a way to deposit a double layer of poly(methacrylic acid)/poly(vinyl pyrrolidone). A similar approach had already been proposed by Zhang et al. [23] and Sochol et al. [24]. This method of "railing" the drops via the addition of obstacles in the flow circuit has also been used to orientate drops in a "pin-balling" manner through different liquids flowing aside each other in a laminar manner without mixing [20,25,26]. Other, more complex devices have been proposed, including the example of magnetic drops [27,28] or a combination of soaking/washing sequences of particles moving through porous fibers permeable to polymer chains [29].

Our goal here is to show that bubbles can be coated directly by PE multilayers in a millifluidic device by exploiting their buoyancy to guide them through different liquid flows. We aim at combining in a single millifluidic Lab-on-a-Chip the generation of monodisperse bubbles of controlled size and spacing with a layer-by-layer deposition of oppositely charged polyelectrolytes. For this purpose, as sketched in Fig. 1a, we set up an original "stratified" millifluidic system (each chip counting as a stratum of the system), composed of a vertically aligned stack of identical chips containing each a serpentine channel. As shown in Figs. 1 and 3, the setup is designed such that continuously flowing polyelectrolyte solutions of NaPSS and poly(allylamine chloride) (PAH) alternate between consecutive strata, which can be piled up to an arbitrary number. The specificity of this setup is that it allows to create bubbles in the bottom chip, and to make them flow slowly along the channel before they rise up to the next chip by gravity. In each chip, a specific polyelectrolyte adsorbs to the bubble surface. For the first NaPSS layer, this adsorption is driven by the amphiphilic properties of NaPSS, [30–35], while for the following layers, the adsorption is driven by electrostatic interactions. Thus a "layer-by-layer" polymeric skin is formed at the interface (Fig. 1b), creating a multilayer gas capsule and stabilising the bubbles against coalescence. We provided recently an in-depth investigation of the formation and mechanical properties of these multilayers on isolated bubbles and interfaces [35].

As shown in Figs. 1a and 2, the bubbling is performed in the bottom chip by injecting nitrogen at constant pressure P_G into the channel through a horizontally held dispense tip of circular cross-section of radius R_N. A cross-flow condition is created by the liquid flowing at constant flow rate Q_L through the channel which detaches the bubble from the tip. The dispense tip is significantly smaller than the channel cross-section D_C (i.e. $R_N \ll D_C$) to reduce interference between the overall liquid flow and the bubbling. The distance D_N between the dispense tip outlet and the opposing channel wall is varied to control the bubble size, while the gas pressure is varied to control the distance D_B between neighbouring bubbles. The effect of each parameter on the bubbling process is investigated in detail in Section 3.

We inject NaPSS solutions in the odd-numbered chips and PAH solutions in the even-numbered chips. The main challenge of this work is to allow bubbles to travel progressively through the different chips without mixing the polyelectrolyte solutions around them. This is ensured by equipping each stratum with an inlet and an outlet for the solution flow and with a vertical connection that allows the bubbles to pass from the lower to the upper stratum by gravity (Figs. 2 and 3). We avoid the formation of polyelectrolyte complexes in the solution around the bubbles by ensuring that the liquid pressure at the connection in the upper channel is systematically higher than the one in the lower channel. In this way a small liquid flow is created against the rising bubble and complexation occurs only in the lower chip in the part of the channel not containing bubbles and leading to the outlet. To obtain the desired flow conditions, we tune explicitly the flow resistance of the channel outlets. To guide this optimisation, we model the flow circuits in analogy with electrical circuits (Section 4).

In the optimised system, the bubbles rise progressively through four strata and are therefore coated with a PSS/PAH/PSS/PAH multilayer at the end. They are then collected at the top outlet of the millifluidic setup and we perform a first preliminary analysis of their properties (Section 4.2).

2. Materials and methods

2.1. Materials

NaPSS (M_w = 77.8 kg/mol, polydispersity index = 1.9) was obtained from Acros Organic, PAH (M_w = 12.5 kg/mol) from Sigma Aldrich, polyethylenimine (PEI, M_w = 60 kg/mol) from Sigma Aldrich, NaCl from Roth. The sulfonation degree of NaPSS was ca. 75% as measured by elemental analysis and by NMR. NaCl was purified by oven pyrolysis at 600 °C for 4h [33]. Details of the in-house characterisation are provided in the Electronic Supplementary Information of a previous paper [35].

We used Milli-Q water from an EMD Milli-Q Direct 8 (Merck Millipore) device to prepare the solutions. Each polymer in solid form is poured together with the salt ([NaCl] = 0.15 M) and the appropriate

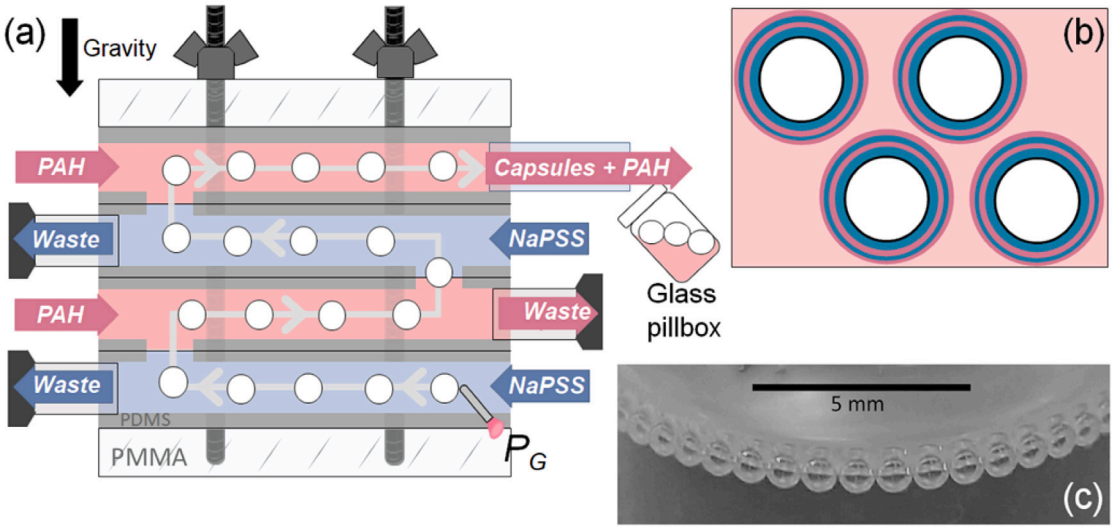

Fig. 1. (a) General principle of the approach: Monodisperse bubbles are generated by injecting nitrogen at constant gas pressure P_G into a flowing solution through a circular dispense tip. Driven by the liquid flow and by gravity, the bubbles rise progressively to the top of a millifluidic device composed of different chips (here four) communicating by a cylindrical connection of the order of 2–3 times the bubble size. Each chip contains a long serpentine channel (about 1 m) hosting the flow of a different solution, here in an alternating manner PSS/PAH/PSS/PAH. The liquids are injected into each layer at constant flow rate Q_L, and each layer contains an outlet. By controlling the flow resistance at the outlets, the flows in the chip are adjusted so that bubbles always move upwards between the chips, while each solution remains mostly within its own chip. Only small flows of the solutions down to the previous chip are allowed so that complexes formed between oppositely charged polyelectrolytes do not enter in contact with the bubbles and are evacuated immediately. (b) Sketch of the obtained bubbles coated in an alternating manner. (c) Example of multi-layer-coated bubbles obtained in the experiments.

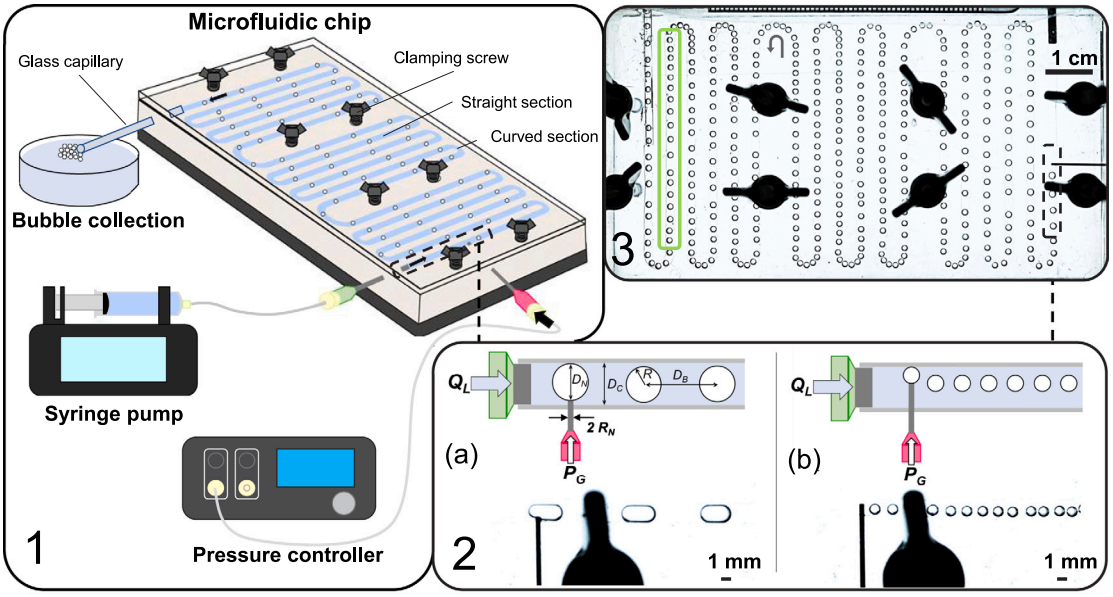

Fig. 2. (1) Sketch of the bottom chip in the configuration used to study the bubbling process. (2) (top) Sketch of the bubbling process with the definition of the main parameters: D_N distance from the tip to the channel wall, D_C channel width, D_B distance between bubbles, R radius of the bubbles, Q_L flow rate of the polyelectrolyte solution, P_G nitrogen pressure, R_N inner radius of the tip, (bottom) corresponding photographs (the black parts are a shadow of a clamping screw). (a) and (b) correspond to large and small values of D_N, respectively, for the same gas pressure P_G. (3) Image of the bottom chip in steady bubbling regime, the green frame shows the region of interest where the image analysis is performed to measure R and D_B.

quantity of Milli-Q water into a volumetric flask. After flushing argon in the flask, the solution is left to stir with a magnetic stirrer at 360 rpm for 12 h at room temperature. After solubilising the salt and polymers, the volume is corrected to the gauge, the pH is lowered at 4.00 ± 0.01, and the solutions used for up to 15 days. We used a concentration of 0.1 g/L in all chips except the bottom one, for which a concentration of 1 g/L was used to accelerate the adsorption kinetics of the first layer [33–35]. We worked at low pH value to increase the charge density of the PAH and favour the electrostatic interaction between layers. Moreover the reproducibility of the experiments is better at this pH value because no ageing effect on the stock solutions induced by water carbonation is observed.

2.2. Millifluidic chip fabrication

The full millifluidic chip consists of stacked, nearly identical PDMS chips with integrated channel systems, as shown in Figs. 1–3. The mold of these chips was drawn with Solidworks, machined in 9 mm thick poly(methyl methacrylate) (PMMA) sheets with a micro-milling machine (Minitech Machinery, software : Mach 3, Endmills) from

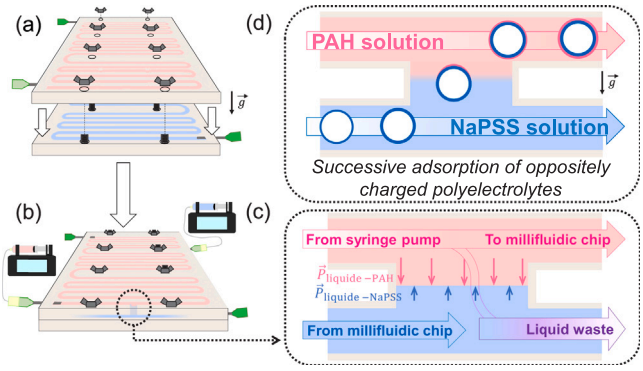

Fig. 3. Scheme showing (a) the stacking of two identical chips rotated by 180°, allowing the alignment of their vertical cavity (b). The flow in both chips is in the same direction (c). By properly tuning the pressure drops in the two chips through the hydrodynamic resistance of the outlets, the bubbles are expected to rise by gravity through the cavity without mixing of the two different solutions in the upper chip (d).

Performance Microtool (reference TS-2-0390) at 10,000 rpm with an overlap rate of 10 percent. The mold has the overall dimensions of 110 × 60 × 5 mm and contains principally a serpentine channel of rectangular cross-section (width: 2 mm, height: 1.5 mm). In two locations of the chip, the spacing between the straight sections of the channel is widened to allow incorporation of two parallel rows of four equidistant pads (height: 5 mm, diameter: 3 mm), forming later holes for clamping screws. At the center of the straight end of the channel, a 3 mm high pad (diameter: 2 mm) is machined to create a communicating passage between the chips.

For the mold of the bottom chip, where gas input is required, a hole is drilled horizontally from the side at the centre of the straight beginning of the channel. This hole allows the insertion of a thin dispense tip perpendicular to the channel. The resulting hole in the bottom chip wall will provide later the entry for the dispense tip that bubbles nitrogen into the chip.

The final chips are made by pouring a mixture of poly(dimethylsilo xane) (PDMS) (Sylgard 184 kit, Dow Corning; ratio of 10:1) into the PMMA mold (rinsed with isopropanol prior to use) and by curing it at 60 °C in the oven for two hours. After demolding, one extremity of the channel is pierced with a drill bit of 1 mm (KAI Medical) to insert a dispense tip (Nordson EFD, Gauge 18) which serves for the injection of liquid. For the exit of the liquid, the other end of the channel is pre-pierced with a dispense tip (Terumo, Nr. 18, 0.45 × 23 mm) to insert later dispense tips of different cross-sections depending on the experimental requirements.

For the bottom chip, a dispense tip with the same diameter as the one used for gas injection is placed in the lateral hole of the mold provided for this purpose before PDMS curing and removed before demolding.

For the assembly, as shown in Figs. 1–3, we place first the chip with the gas input on the PMMA base. The following chips are placed on top of each other in an alternating fashion, each time rotated by 180°, with the engraved face upwards. The top chip is covered by a 1–2 mm thick PDMS film to ensure water tightness. The set-up is then sealed with the second PMMA plate screwed with clamping nuts.

The inlet of each chip is connected to a 60 mL luerlock syringe (BD Plastipak) mounted on a syringe pump (Harvard PhD Ultra) for liquid injection at constant flow rate (1 mL/min). For the injection of nitrogen at constant pressure, a dispense tip (Nordson EFD, Gauge 25) is connected from a pressure controller (Elveflow, OB1 MK3+) into a hole of the bottom chip designed for this purpose. The vertical position of the tip is fixed in the centre of the channel, while its horizontal position inside the channel is varied with a micrometre screw (PT series, Thorlabs) to control the bubble size, as shown in Fig. 2.2. For each chip, waste flow takes place through calibrated dispense tips (Nordson EFD) of various diameters and lengths to control the flow resistance and hence the associated pressure drop across the tip. The length of the tips is adjusted with a disk saw IsoMet™ equipped with a cutting disk Isocut CBN-HC.

Finally the bubbles are collected at the outlet of the upper chip through a glass capillary (diameter: 1.5 mm, Hirschmann) into a glass pillbox (pre-filled with the solution flowing from the glass capillary). The pillbox is tilted at an angle of around 45°, so that the droplets flow directly from the glass capillary into the solution.

To avoid the bubbles sticking to the microfluidic channel walls, the surfaces are made hydrophilic via a treatment adapted from Ref. [36]: The inside of the channel is filled alternately with a PEI solution (2.5 g/L) and a NaPSS solution (1 g/L) for 30 min, and dried with nitrogen between each soaking time. This procedure is repeated six times to create a stable multilayer on the channel surfaces. According to our experience, this treatment remained hydrophilic for more than 15 days.

2.3. Imaging and image treatment

The millifluidic chip assembly is placed on a light panel (Wafer 1 Daylight) to provide optimal lighting for a good outline of bubbles inside the channel. A camera (Canon, EOS 850D) is placed 80 cm vertically from the millifluidic assembly to take images. We use the "particle analysis tool" of *ImageJ* software [37,38] to detect the bubbles in the channel by setting the software to identify and analyse objects within a specific size and circularity range. After scaling, we extract the area A_B and the position of each bubble in different zones of the chip. The final analysis was performed on the last straight section of the channel (green frame in Fig. 2.2). We then use an *Excel* macro to obtain the interbubble distance D_B from the center positions. To obtain the average bubble radius $\langle R \rangle$, we distinguish between two cases. If the bubbles are smaller than the channel depth, they are spherical and we use the following formula to calculate the bubble radius $R = \sqrt{A_B/\pi}$. If the bubbles are larger than the channel depth, they form elongated "slugs" whose geometry is complex when $2R \approx D_C$ [39]. Since we are not quantitatively interested in this regime, we use here a simple approximation of the bubble cross-sections as ellipses and obtain the equivalent radius of the bubble as $R = 2A_B/\pi D_C$, considering that the small axis length is D_C.

2.4. Flow rate measurements

The liquid flow at the exit of each chip is measured by weighing the mass of solution flowing for 5 min from the outlet in steady flow conditions, after a stabilisation time of 3 min.

3. Bubbling investigations

We investigate first the bubbling conditions in the bottom millifluidic chip to produce monodisperse bubbles with controlled bubble radius R and interbubble distance D_B, as sketched in Fig. 2.2.a. For the bubble size, we aim for bubbles smaller than the channel width D_C in order to ensure a spherical bubble shape and homogeneous deposition of polyelectrolytes on the bubble surface. Yet, the bubbles should not be much smaller than D_C in order to be carried along efficiently and homogeneously by the liquid flow [40]. The conditions sought for the interbubble distance D_B also ask for a compromise: D_B needs to be large enough to avoid coalescence and hydrodynamic interactions between bubbles, yet it should be small enough to maximise the number of bubbles per liquid volume used.

As shown in Fig. 2, bubbles are produced by cross-flow generation around a circular tip of radius R_N inserted into the millifluidic channel of nearly square cross-section of width D_C (Section 2.2) with $2R_N/D_C = 0.29$. To control the bubble size at constant flow conditions, we vary in a controlled manner the distance D_N between the tip outlet

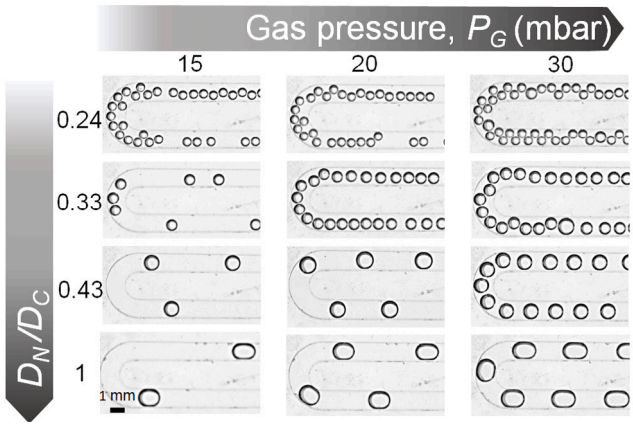

Fig. 4. Evolution of the bubble configuration in the channel for increasing distance between the tip outlet and channel wall D_N/D_C (top to bottom) and for increasing gas pressure P_G (from left to right) in the first chip (Fig. 2) in NaPSS solution at Q_L = 1 mL/min.

and the channel wall, as sketched in Fig. 2.2. This is different from most previous work reported in the literature, where the variation of the bubble size is achieved via the variation of gas pressure P_G and liquid flow rate Q_L at fixed channel geometry [41–43]. The use of tunable channel geometries has been reported [6,7,44], but there the full channel cross-section is varied.

In this work, we choose for simplicity to keep Q_L constant at 1 mL/min and to vary only the relative tip position D_N/D_C and the gas pressure P_G to control R and D_B. After determining D_N by image analysis, we start bubbling. When the entire channel is filled with a homogeneous train of bubbles, we wait five minutes to ensure that the flow conditions are stable. We then start taking photographs at regular intervals so that each photograph contains a new set of bubbles. In order to ensure good statistics we take enough photographs to measure at least 200 bubbles each time.

Fig. 4 shows typical photographs of bubble trains obtained for different D_N/D_C and P_G. One notices first of all that bubbles of very different sizes can be generated : from sub-millimetric, spherical bubbles for small D_N/D_C to slugs (bubbles deformed by the channel geometry) for large D_N/D_C.

We observe two trends. For a fixed value of P_G, the larger D_N/D_C the larger R and D_B. On the contrary, for a fixed value of D_N/D_C, the larger P_G, the smaller D_B. If D_B is too small, bubbles start touching each other and one observes occasionally coalescence. Overall, P_G does not seem to impact significantly R. One also notices, that for smaller bubbles, the interbubble distance D_B becomes quickly irregular due to hydrodynamic instabilities of the bubble flow.

Using image analysis (Section 2.3), we quantified these different observations. Fig. 5a shows how the average, reduced bubble radius $2\langle R\rangle/D_C$ varies with D_N/D_C for different gas pressures P_G: there are two very different bubbling regimes, depending on the bubble size. In the first regime, when the bubbles are smaller than the channel cross-section ($2\langle R\rangle/D_C < 1$), the bubble radius grows linearly up to $D_N/D_C \approx 0.5$. In this regime, to first approximation, the bubble size is independent of the gas pressure P_G. In the second regime, on the contrary, when the bubbles are slugs ($2\langle R\rangle/D_C > 1$), the bubble size is to first approximation constant with D_N/D_C but depends instead non-negligibly on P_G.

We explain the existence of these two regimes as follows. In the first regime, bubble blowing takes place in the "dripping regime" [41], i.e., the bubbles detach from the tip when the viscous drag exerted by the liquid flow around the bubble overcomes the capillary forces which

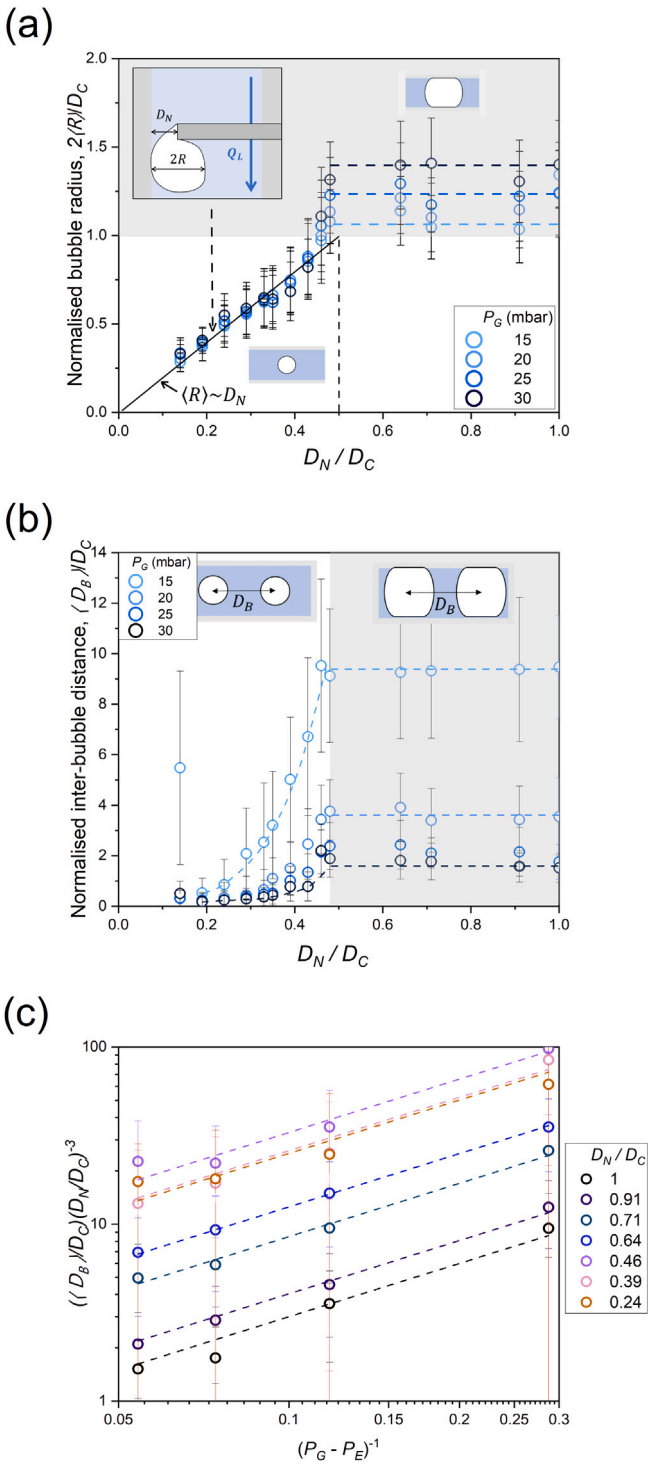

Fig. 5. Variation of (a) reduced average bubble radius, $2\langle R\rangle/D_C$ and (b) reduced average interbubble distance $\langle D_B\rangle/D_C$ as a function of reduced tip position D_N/D_C for different gas pressures P_G; (c) Data in (b) replotted using the scaling of Eq. (7). Bubbles are created in a NaPSS solution at flow rate Q_L = 1 mL/min.

attach the bubble to the tip. For these kind of detachment conditions one typically finds that [41]

$$R \propto \frac{\gamma}{\eta U} L, \tag{1}$$

where γ is the surface tension, η the viscosity of the liquid, U a characteristic flow velocity and L the characteristic length scale of the flow. In our problem, $L \propto D_N$, while all other quantities are to first approximation constant, hence $\langle R \rangle \propto D_N$. The prefactor of this relation depends on the flow geometry, which is complex in our case, since the tip only takes up a part of the channel cross-section. However, one notices that the solid black line in Fig. 5a corresponds geometrically to the situation where the bubble is dragged by the flow slightly downstream of the tip and detaches as soon as it touches the channel wall on the other side, as sketched in the inset of the same figure. We believe that this geometric condition facilitates the topological change at the needle tip that initiates the detachment. This condition corresponds to the relationship

$$\frac{2R}{D_C} \approx 2\frac{D_N}{D_C}, \tag{2}$$

which captures nicely the data (black line in Fig. 5a) and which we will use in the following. Future work will have to investigate this regime more deeply to establish the quantitative influence of all process parameters.

In the second regime, the bubbles are squeezed by the channel walls, creating quickly flow conditions which correspond to the "squeezing regime" [41]. Here the bubble blocks the channel and hence the break-up mechanism is dominated by the pressure conditions. Globally, one finds to first order for these regimes that [41,45,46]

$$\frac{2R}{D_C} \propto \left(1 + C\frac{P_G}{Q_L}\right), \tag{3}$$

since the bubble size is fixed by the time it takes to fill the constriction holding the bubble to pinch it off. The prefactor depends again on the channel geometry and the constant C is related to the hydrodynamic resistance of the gas flow. Since the bubble already blocks the entire channel, the tip position becomes less relevant in this regime. Since Q_L and D_C are constant, we recover a linear dependency of the bubble size on P_G (Electronic Supplementary Information, Fig. S1)).

Let us now consider the normalised mean distance $\langle D_B \rangle / D_C$ between bubbles. This is shown in Fig. 5b as a function of the needle position D_N/D_C for different P_G. One notices again the same two regimes. In the first regime, $\langle D_B \rangle / D_C$ depends strongly on the needle position, while in the second regime it remains constant. In both regimes, $\langle D_B \rangle / D_C$ depends on the gas pressure P_G. To explain this observation, let us consider the first regime, in which the mean bubble size $\langle R \rangle$ is independent of P_G (Fig. 5a). Then, D_B is entirely fixed by how much time it takes to create a bubble of volume V. Using an average gas flow rate Q_G and an average liquid velocity of roughly Q_L/D_C^2, we can write

$$D_B = \frac{V}{Q_G}\frac{Q_L}{D_C^2}. \tag{4}$$

In order to relate Q_G to P_G, we notice that the system has an entry pressure P_E which needs to be overcome to inject the gas into the channel through the small tip of radius R_N. This entry pressure corresponds to the maximum Laplace pressure arising during bubble formation, i.e., when the bubble is a hemisphere of radius R_N, given by

$$P_E = \frac{2\gamma}{R_N}. \tag{5}$$

Since the NaPSS does not have enough time to adsorb during the rapid bubbling process [35], we use the surface tension of water ($\gamma = 72$ mN/m) and $R_N = 0.125$ mm to find $P_E \approx 12$ mbar. This corresponds to our experimental observations since we have to use $P_G \geq 15$ mbar to create bubbles in the system.

We can assume that the flow resistance of the gas in the circuit before the tip is constant and that therefore $P_G - P_E \propto Q_G$. We then obtain that

$$\frac{D_B}{D_C} \propto \frac{R^3}{D_C^3}\frac{Q_L}{(P_G - P_E)}. \tag{6}$$

Using Eq. (2), this can be simplified to

$$\frac{D_B}{D_C}\left(\frac{D_N}{D_C}\right)^{-3} \propto (P_G - P_E)^{-1}. \tag{7}$$

In Fig. 5c this scaling was used to fit the experimental data and is represented by the dashed lines. It shows that this scaling captures indeed well the inverse proportionality with the pressure difference $P_G - P_E$ for all data - keeping in mind, that the investigated pressure range is rather small. It also collapses well the data in the first regime ($D_N/D_C < 0.5$), for which Eq. (7) was derived. In the second regime ($D_N/D_C > 0.5$), the data is nicely collapsed by the simple scaling $D_B/D_C \propto (P_G - P_E)^{-1}$ (Electronic Supplementary Information, Fig. S2), since the bubble size is, to first approximation, independent of the position of the dispensing tip.

To summarise, we find a highly reproducible bubbling behaviour with two distinct regimes. The first regime corresponds to a "dripping regime", where the bubbles are smaller than the channel cross-section and they are detached from the tip by viscous forces. Since the liquid flow rate is constant, the bubble size depends only on the tip position D_N/D_C in the channel and is given by Eq. (2). The gas pressure P_G influences only the distance D_B between the bubbles, the relevant scaling being given by Eq. (7). The second regime corresponds to one where the bubbles are larger than the channel cross-section leading to a "squeezing-type" flow controlled by the pressure conditions in the channel. Here the bubble size depends negligibly on the tip position but increases linearly with gas pressure P_G.

In the following, we choose the bubbling conditions P_G and D_N such that $2\langle R \rangle \simeq 0.75\ D_C$ and $\langle D_B \rangle \simeq 5\ D_C$, which satisfy the requirements discussed at the beginning of this section.

4. Layer-by-Layer deposition

We want to design a millifluidic device allowing the bubbles to move from one polyelectrolyte solution to the next in an alternating manner, each time spending enough time in the solution to be covered by the respective polyelectrolyte. As briefly discussed in Section 1, this is achieved by making the bubbles travel along each chip of the device, with alternating polyelectrolyte solutions, the first being NaPSS in the bottom chip. Neighbouring chips are connected by a vertical passage that allows the bubbles to rise into the next chip via gravitational forces. Unfortunately, these passages can also allow liquid to pass, leading to undesired mixing and aggregation of the polyelectrolyte solutions. Ideally, the pressures of both liquids would be identical at the passage in order to avoid liquid exchange (Fig. 3c). However, the high flow resistance of the bubbles introduces important pressure fluctuations that destabilise the overall flow conditions. We therefore design the system to allow for the mixing of the solution but only in parts of the channel system not containing bubbles, i.e, the pressure conditions are optimised such that at each passage the liquid pressure in the upper chip is slightly higher than in the lower one, creating a small liquid flow downwards (against the bubble motion). Liquid mixing occurs then in a part of the channel without bubbles whose liquid flow is carried directly to the waste bin (see "waste" in Figs. 1 and 3c).

To create the desired pressure conditions, we tune the hydrodynamic resistance of the exit of each chip by adjusting the length and diameter of the narrow dispense tip that makes the outlet. We aim at downward flows in all passages of the setup requiring that they are small enough to not hamper the rise of the bubbles against them.

Since the flows in the different chips are highly coupled and depend also on the flow resistance of the bubbles, we investigate first in depth the flow between two chips, initially without bubbles, then with a steady train of bubbles (Section 4.1), before moving on to a setup with four chips (Section 4.2).

4.1. Two chips

Here we work with the first two chips only, the first one containing the bubbling process (Section 3). The liquid injection rate Q_L in each chip is kept constant at $Q_L = 1$ mL/min throughout the entire experiment. We can draw the overall flow circuit as sketched in Fig. 6a, associating a flow resistance with each channel part and exit dispense tip. In the upper chip (2), liquid and bubbles exit through a circular glass capillary of 1.5 mm inner diameter and approximately 15 mm length with an associated flow resistance $R_{out,2}$ (Fig. 6a). In addition, the liquid (and bubbles) probe also the hydrodynamic resistance of the whole channel, R_C of ca 1 m length. The liquid of the bottom chip (1) exits through a narrow dispense tip whose diameter and length are adjusted to tune the flow resistance $R_{out,1}$. The outlet channel is very short (≈ 20 mm), so that we can neglect its hydrodynamic flow resistance with respect to that of the tip. Before reaching the passage of flow resistance R_P, liquid and bubbles have probed the channel resistance, R_C, and the resistance from its inlet, $R_{in,1}$.

As the chips communicate through the vertical passage, varying the flow resistance of the outlet of the lower chip will impact not only the associated exit flow rate $Q_{out,1}$ in this chip, but also the exit flow rate $Q_{out,2}$ of the upper chip. Overall we know that

$$2Q_L = Q_{out,1} + Q_{out,2}, \tag{8}$$

since the overall flow rate is conserved. Using Kirchhoff's laws for pressure drop and conservation of flows across each channel section, we can write for the circuit $A - B - C - D$ on the right of the passage

$$(P_A - P_B) + (P_B - P_C) + (P_C - P_D) + (P_D - P_A) = 0, \tag{9}$$

$$Q_{P,1} + Q_L = Q_{out,1}. \tag{10}$$

Since both outlets are at atmospheric pressure, $P_B - P_C = 0$. Moreover the pressure drop $P_D - P_A$ due to the hydrodynamic resistance of the passage is partly compensated by the hydrostatic pressure difference between the two neighbouring chips, $P_D - P_A = R_P\, Q_{P,1} - \Delta P_H$, and Eq. (9) becomes

$$R_{out,1}\, Q_{out,1} - (R_{out,2} + R_C)\, Q_{out,2} + R_P\, Q_{P,1} - \Delta P_H = 0, \tag{11}$$

where $\Delta P_H \approx 50$ Pa is estimated from the geometry of the device. Since the passage is very short and wide, and the flow between the two strata, $Q_{P,1}$, should be small compared to $Q_{out,1}$, we can neglect the term $R_P\, Q_{P,1}$ in Eq. (11). Setting $q_i = Q_{out,i}/Q_L$, Eqs. (8) and (11) can then be rearranged as

$$q_1 + q_2 = 2, \tag{12}$$

$$R_{out,1} q_1 - (R_{out,2} + R_C)\, q_2 = R_0, \tag{13}$$

where $R_0 = \Delta P_H / Q_L \approx 3$ Pa s/mm^3 is an effective resistance related to the hydrostatic pressure difference between two neighbouring chips. From Eqs. (12) and (13), we obtain

$$q_1 = \frac{R_0 + 2(R_{out,2} + R_C)}{R_{out,1} + R_{out,2} + R_C}. \tag{14}$$

Then $q_1 - 1 = (Q_{out,1} - Q_L)/Q_L = q_{P,1}$ is the normalised flow in the passage and is positive (resp. negative), when this flow is directed downwards (resp. upwards).

To test this relation, we performed a series of experiments, varying systematically $R_{out,1}$ and measuring $Q_{out,1}$ in the absence and in the presence of bubbles, using the bubbling conditions chosen at the end of Section 3 ($\langle R \rangle = 0.70 \pm 0.05$ mm and $D_B = 15 \pm 5$ mm). In Fig. 6b we plot $q_{P,1}$ for both cases as a function of $R_{out,1}$, which we estimated using Hagen–Poiseuille's law for pipes with circular cross-section

$$R_{out,i} = \frac{8L\eta}{\pi a_N^4}, \tag{15}$$

where L and a_N are the length and the inner radius of the dispense tip, and $\eta \approx 1$ mPa s the fluid viscosity. Along with the data we plot the

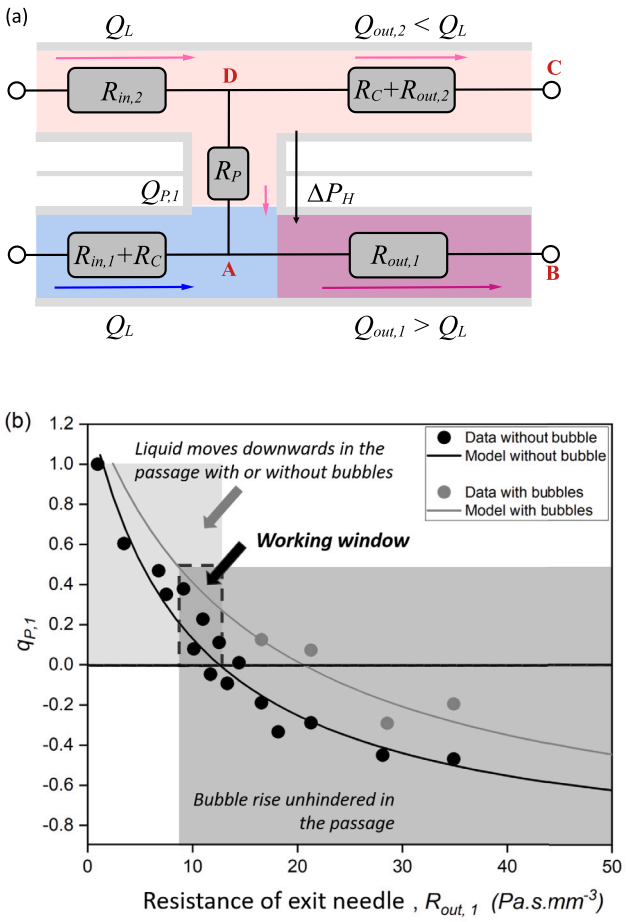

Fig. 6. Optimisation of the flow between the two chips. (a) Schematic representation of the different flow resistances along the channel system. (b) Normalised flow rate through the passage connecting the two chips, $q_{P,1} = (Q_{out,1} - Q_L)/Q_L$, with and without bubbles, as a function of the hydrodynamic resistance across the outlet tip in the bottom chip for $Q_L = 1$ mL/min. The lines are fits using Eq. (14) with (grey) or without (black) bubbles taking the hydrostatic pressure difference between the chips into account. The working window is defined by the conditions that the liquid flow through the passage has to be downward with as well as without bubbles, to avoid mixing in the channels transporting the bubbles; and that this downward flow has to be small enough to avoid interference with the bubble rise and hence coalescence. Experimentally we found that $q_{P,1} < 0.5$ was needed.

prediction of Eq. (14) (solid line) using $R_{out,2} + R_C$ as fit parameter. We see that globally the data are well described by Eq. (14). We obtain $R_{out,2} + R_C \approx 9.6$ Pa s/mm^3 in the case of bubble-free flow and $R_{out,2} + R_C \approx 13.2$ Pa s/mm^3 in the presence of bubbles.

In the case of bubble-free flow we can estimate $R_{out,2} \approx 1$ Pa s/mm^3 using Eq. (15), and $R_C \approx 3.5$ Pa s/mm^3 using the expression of the hydrodynamic resistance of a rectangular duct [47]

$$R_C = \frac{\eta L}{4ba^3}\left[\frac{1}{3} - 2\frac{a}{b}\sum_{n=0}^{\infty}\left(\frac{2}{\pi(2n+1)}\right)^5 \tanh\left(\frac{\pi(2n+1)b}{2a}\right)\right]^{-1}, \tag{16}$$

where $a = 1$ mm and $b = 0.75$ mm are, respectively, the half-width and the half-depth of our rectangular channel, and $L \approx 1075$ mm is its length. Thus the estimated value, $R_{out,2} + R_C \approx 4.5$ Pa s/mm^3, is similar to what we find in the experiment, although Eq. (16) is valid for a straight channel and does not take into account the windings through the chip.

The presence of bubbles modifies strongly the flow conditions and our flow model is likely oversimplified. In particular, it does not take into account the perturbation of the flow in the passage by the bubbles.

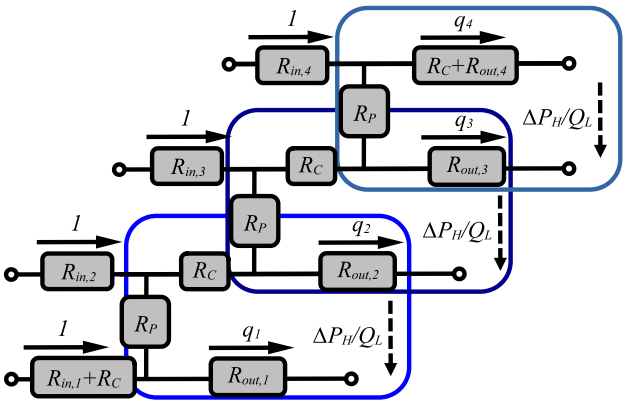

Fig. 7. Scheme of the electrical analogy for the millifluidic device with four chips. All the flows are normalised by the constant input flow rate, $Q_L = 1$ mL/min. The three rounded boxes display the three identical circuits used to write Kirchhoff's laws. These circuits are identical to the one depicted in Fig. 6a.

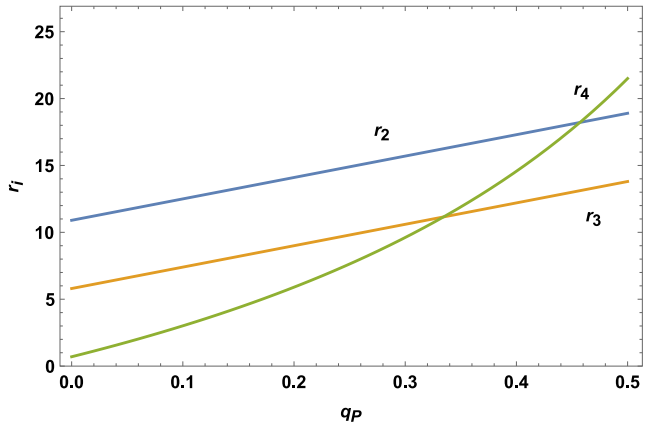

Fig. 8. Values of the normalised hydrodynamic resistances r_2 to r_4 as a function of the normalised flow q_P in the passages between the chips. In Eqs. (27)–(29), we set $r_c = 4.1$ and $r_1 = 16$ to be consistent with the results in Section 4.1 and to obtain positive values for r_4.

This perturbation depends on the bubble size and on the diameter of the passage. Estimating the hydrodynamic resistance of a bubble train is much more involved due to the complex flow-shape interactions of the deformable bubbles [48–50]. However, we note that, as expected, the presence of the bubbles increases measurably the fitted value of $R_{out,2} + R_C$.

We can therefore optimise the flow between two chips as follows: Since we always have to avoid that mixing of solutions occurs in the main channels, we need to identify a range of outlet resistances $R_{out,1}$ in which $q_{P,1}$ is positive in the presence of bubbles. At the same time, $q_{P,1}$ needs to be as small as possible in order to avoid that the downward flow hampers the rising of the bubbles. Estimating the viscous force acting on the rising bubble created by the downward flow, one notices that, in principle, the bubbles should always be able to rise against the downward flow in our conditions. This is due to (1) the large bubble size (strong buoyancy force), (2) the even larger cross-section of the passage, and (3) the low flow rates. However, experimentally we noticed that for $q_{P,1} > 0.5$ the downward flow created enough slowing down at the passage to encourage bubble encounters and hence coalescence. We therefore decided to stay below this value. Both conditions provide an approximative working window for the outlet resistances, as sketched in Fig. 6b.

4.2. Four chips

Since the final device needs to have more than two chips, we work iteratively based on what we learned from Section 4.1. We consider here up to four chips, but the proposed strategy can be extended to an arbitrary number of chips. In the case of four chips the device is the superposition of three passages like the one in Fig. 6a. Its equivalent electrical circuit is displayed in Fig. 7. The boxes delimit the parts of the circuitry used for the calculations. They correspond to the four outlets coupled by the three passages between the four chips. We set $r_i = R_{out,i}/R_0$ and $r_C = R_C/R_0$. Extending Eqs. (12) and (13), we obtain

$$q_1 + q_2 + q_3 + q_4 = 4, \tag{17}$$

$$r_1 q_1 - (r_2 + r_C) q_2 = 1, \tag{18}$$

$$r_2 q_2 - (r_3 + r_C) q_3 = 1, \tag{19}$$

$$r_3 q_3 - (r_4 + r_C) q_4 = 1, \tag{20}$$

We note that the flows in the three passages are given by

$$q_{P,1} = q_1 - 1, \tag{21}$$

$$q_{P,2} = q_1 + q_2 - 2, \tag{22}$$

$$q_{P,3} = q_1 + q_2 + q_3 - 3 \tag{23}$$

with positive values corresponding to downwards flow in the passages. Using Eqs. (21)–(23) and the conservation of flow, Eq. (17), we can express the $\{q_i\}$ as a function of the $\{q_{P,i}\}$, replace them in Eqs. (18)–(20) and then solve for the $\{r_i\}$ to obtain

$$r_2 = \frac{r_1(1 + q_{P,1}) - r_C(1 - q_{P,1} + q_{P,2}) - 1}{1 - q_{P,1} + q_{P,2}}, \tag{24}$$

$$r_3 = \frac{r_1(1 + q_{P,1}) - r_C(2 - q_{P,1} + q_{P,3}) - 2}{1 - q_{P,2} + q_{P,3}}, \tag{25}$$

$$r_4 = \frac{r_1(1 + q_{P,1}) - r_C(3 - q_{P,1}) - 3}{1 - q_{P,3}}. \tag{26}$$

We are interested in quadruplets that yield small positive values of $q_{P,i}$. Moreover we have four unknowns $\{r_i\}$ with only three independent Eqs. (24)–(26) and r_1 can be chosen to ensure that r_4 remains positive. The different sets of possible solutions to Eqs. (24)–(26) can be found numerically. A very satisfying subset of solutions is obtained by requiring that the flow conditions of all passages are identical, i.e, $q_{P,i} = q_P$. Then Eqs. (24)–(26) reduce to

$$r_2 = r_1(1 + q_P) - (r_C + 1), \tag{27}$$

$$r_3 = r_1(1 + q_P) - 2(r_C + 1), \tag{28}$$

$$r_4 = \frac{r_1(1 + q_P) - 3(r_C + 1)}{1 - q_P}, \tag{29}$$

and correspond to flow conditions where the bubbles spend about the same travelling time along each stratum. Indeed the normalised fluid velocity in the part of the channel where bubbles travel is then simply 1 in the bottom chip and $1 - q_P$ in the three upper chips. Fig. 8 shows the values of r_{2-4} as a function of q_P, for $r_C = 4.1$, a value consistent with the fitted value of R_C in Section 4.1, and $r_1 = 16$, a value large enough to ensure that r_4 is positive. Despite the interest of these calculations to prove the existence of satisfying flow conditions and to efficiently search for them, in practice we still had to rely on empirical tuning of the device, especially in the presence of bubbles, which modify a lot the resistance to the flow as a function of their size and number in the different channels, making the calibration provided in Fig. 6b very approximate. We therefore describe now this empirical approach.

Before starting, each chip of the device is filled with liquid. Flow rates q_{1-4} are determined by weighing the volume of liquid flowing from each chip over 5 min. In the four-chip system, $R_{out,4}$, which corresponds to the resistance in the top chip, is constant: the glass capillary is permanently attached to the outlet of the microfluidic channel. Liquid flow between each chip is therefore regulated by varying the

Table 1
Values of the hydrodynamic resistances, of the resulting normalised output flows, and of the corresponding flows through the three passages, without bubbles (wo) or with bubbles (w) present in the four chip device. Note that the $R_{out,i}$ values are calculated by Eq. (15), i.e., in the absence of bubbles, and simply translate the length and diameter of the dispense tips into hydrodynamic resistances. Therefore the effective $R_{out,4}$ in the presence of bubbles is larger than its value in the Table. The other $R_{out,i}$ are not affected: the larger $R_{out,1}$ value in the presence of bubbles reflects simply the use of a dispense tip longer than in the absence of bubbles.

i	$R_{out,i}$	Without bubbles		With bubbles	
	(Pa s mm^{-3})	q_i	$q_{P,i}$	q_i	$q_{P,i}$
4	9.7	0.90	–	0.88	–
3	13.3	1.09	0.1	1.12	0.14
2	18.2	1.02	0.01	1.15	0.02
1	35.2$^{(wo)}$, 43.2$^{(w)}$	0.99	−0.01	0.87	−0.13

$R_{out,i}$ resistances with $i = 1-3$, by inserting tips of adjustable gauge and length into the corresponding chip using a top-down flow control method.

Since $R_{out,4}$ is kept constant, the liquid inlets and outlets of the bottom two chips are plugged to start regulating flows q_3 and q_4. Looking at the working window of Fig. 6b, the condition to be met is about $0.9\, q_i < q_{i+1} < q_i$ to ensure that there is no liquid rising from the lower chip to the upper chip. Once flows q_3 and q_4 are satisfactory, the second chip is connected to the syringe pump, $R_{out,2}$ adjusted and the measurement repeated until the condition is met between q_2 and q_3, while remaining valid between q_3 and q_4. Finally, this procedure is repeated a third time to include and regulate q_1, by adjusting $R_{out,1}$, while still respecting the above-mentioned condition.

Table 1 shows the final values of the $R_{out,i}$, the resulting output flows for the four chips of the device, and the corresponding flows in the three passages between the chips. These values are considered satisfactory, because if the condition is not perfectly met between chips 1 and 2, the liquid flow rate $q_{P,1}$ rising in chip 2 is less than 0.01. The assumption is that, as this quantity is reasonably small, the multilayer deposition of PE chains should not be affected. This experiment shows that it is necessary to gradually increase the value of $R_{out,i}$ while using this top-down flow control method to regulate liquid flows as is done here. Additionally to the flow rate measurements, visual observation of the liquids in the channel and the liquid surrounding the bubbles collected in the container allows to detect potentially undesired mixing: the mixing of the solutions of oppositely charged polyelectrolytes created aggregates leading to a turbid solution and to aggregates settling around the bubbles in the container which are easily observable if the flow conditions are not optimised. Under optimised conditions, these aggregates are detected only in the waste containers.

Once satisfactory liquid flow parameters have been found without bubbles, the experiment is repeated in the presence of bubbles in the device, following the bubbling conditions defined in Section 3. The presence of bubbles in the microfluidic channels significantly disturbs the liquid flow in each chip. Table 1 shows the most optimal q_i flows obtained by the top-down flow control method. Despite the fact that $R_{out,1}$ has been increased in the presence of bubbles to compensate the pressure increase in the device, the liquid flow rate $q_{P,1}$ rising in chip 2 is now $q_{P,1} \approx 0.13$. Under these conditions, the deposition of the first two PE layers ([PSS/PAH]) is therefore expected to be disrupted by the mixing of the liquid phases and the formation of PE aggregates in solution. Nevertheless, as a proof-of-concept, we present and analyse one of the obtained samples in Section 4.3. A movie showing the device operating in steady mode is available in the Electronic Supplementary Information.

One drawback of our current design is the use of PDMS to make the chips. This introduces a large sensitivity of the device to the pressure exerted by the clamping screws. Therefore it is difficult to reproduce the values of R_C due to the deformability of the PDMS parts upon tightening the device. Future improvements will use harder chip materials to replace the PDMS parts.

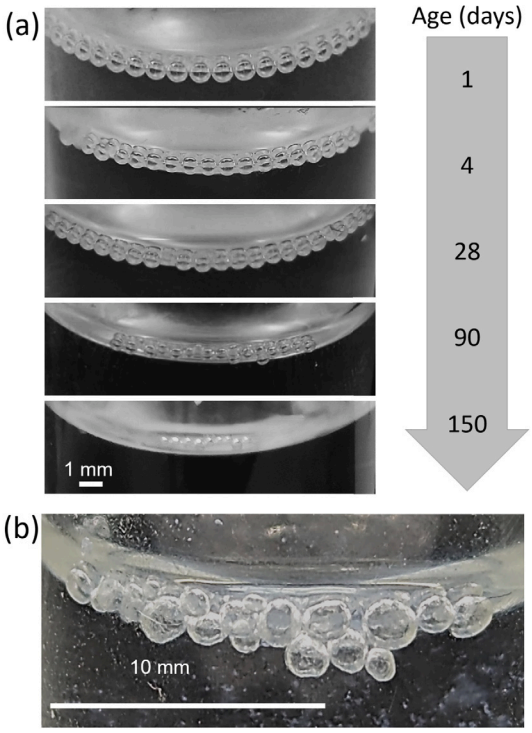

Fig. 9. (a) Evolution of multilayer capsules with four layers [PSS/PAH/PSS/PAH] generated with the setup containing four chips and the conditions listed in Table 1. (b) Example of non-spherical bubbles after four months.

Clearly more work is needed to optimise the flow conditions in the presence of bubbles. In particular, we need to take into account the differences in flow resistance due to the varying number of bubbles in the chips, which results from their different flow rates. Therefore systematic measurements of the contribution of bubbles to the flow resistance should be performed as a function of their number and size, i.e., of the bubbling conditions, and also of their surface properties (a bubble covered by a polyelectrolyte multilayer will influence the flow resistance differently to an uncovered bubble due to the change in slip-conditions on its surface). Then chip-dependent $R_{C,i}$ values could be introduced in the r_i definition. This is out of the scope of the present paper, which aimed to introduce a proof-of-concept for a device allowing the adsorption of multilayers on bubbles or droplets. Moreover, future designs should consider a more flexible method of tuning the outlet resistances.

4.3. First analysis of multilayer bubbles

Monodisperse spherical bubbles are obtained and collected without manual intervention as explained at the end of Section 2.2. We observe that they remain completely stable against coalescence only after deposition of the fourth PE layer, showing the importance of the multilayer properties to fully stop coalescence (Fig. 9a). The collected bubbles gather at the glass wall of the container and their size and number decrease slowly with time due to the higher pressure of the gas inside the bubbles. A preliminary photographic study was carried out to measure the decrease of the average bubble diameter with time (Fig. S3 in Electronic Supplementary Information). The speed at which the bubbles shrink appears to decrease with time but after five months a majority of bubbles has disappeared. The observed time scales of the

bubble dissolution are orders of magnitude larger than those observed for bubbles stabilised by simple polymeric surfactants. The latter tend to be of the order of hours rather than months, thus indicating the presence of a PE layer with elastic properties [51]. A compacting PE layer can also provide some resistance to the gas diffusion [14]. In previous work [35] we showed that the formulation used in this article creates multilayers with a liquid-like elastic response up to four PE layers, indicating the presence of multilayer islands which can still be re-rearranged and compacted and hence allow for reduction of the bubble surface required for gas dissolution. The fact that gas dissolution does not fully stop after some time (Fig. 9) indicates that the islands can still detach under the compression of the bubble dissolution. In some cases we observed much less bubble shrinkage combined with non-spherical bubble shapes (Fig. 9b), indicating a progressively solid-like layer due to the compaction of the islands. Obtaining such a solid-like multilayer directly after multilayer deposition is expected only from the fifth layer onwards, as we showed in [35]. Hence, bubbles would then be expected to be stable also against dissolution. These different interpretations are still working hypothesis since at this stage we lack direct structural characterisation of the interfaces to confirm that we construct indeed multi-layers at the interface. In principle, our design ensures that the formation of polyelectrolyte complexes and their adsorption on the bubbles can only occur in the passage between chips, i.e., during a very short time compared to the travelling time in the chips. However, if needed, intermediate chips circulating brine can be added to include a washing step between adsorption steps. Last but not least, our work in [35] has put in evidence the high sensitivity of the multilayer properties to the deposition and manipulation protocol, which are quite different under the millifluidic flow conditions in comparison to the single-bubble experiments performed in [35]. More systematic work and quantitative characterisation of the obtained bubbles - and their interfacial properties - are therefore needed to establish quantitative correlations. Nevertheless, we think that the provided results show the general potential of the method.

5. Conclusion and outlook

We introduced a new millifluidic device that produces monodisperse bubbles with tunable size and spacing, and that uses buoyancy to drive them through superposed chips with different circulating fluids.

Two elements in this design are new and expected useful for a wider community. Firstly, we resolve the problem of decoupling bubble size, bubble spacing and the flow conditions by injecting gas through a small and movable dispense tip into the cross-flow of the solution through a rectangular channel. We investigate the effect of the position of the tip outlet, proving a fine and reproducible control over the bubble size and spacing over a wide range. While we provide some first hypotheses of the acting mechanisms, more systematic work needs to be done in the future to capture the impact of all system parameters, including the liquid flow rate or the needle radius.

Secondly, the original design exploits the buoyancy of the bubbles to make them move through successive strata containing different polyelectrolyte solutions for the successive adsorption of different constituents onto the bubbles and the building of functional multilayer capsules. Our proof of concept was done with the example of four polyelectrolyte layers, which endow the bubbles with an exceptional longevity. However the device can be easily adapted to a larger number of layers and more complex architectures, including the addition of washing steps. The bubbles can also be replaced by solid particles or drops, provided that their density is sufficiently different from that of the surrounding liquids to exploit buoyancy.

We provided the general method to optimise the flows in the chips to allow the uprising of the bubbles between chips while preventing the mixing of the different fluids in the parts of the circuitry where bubbles are present. While our analysis of bubbles passing through a four-layer chip proves the progressive deposition of polyelectrolytes on the bubble surface, structural characterisation of the obtained layers needs to prove their multilayer nature in future work.

Future necessary improvements of the device will involve the use of harder chip materials and a more flexible control over the outlet resistances coupled with a more quantitative understanding of the hydrodynamic resistance of the circulating bubbles. Alternatively, one may consider controlling directly the outlet flow rates.

Apart from the fundamental interest of providing a proof of concept of the millifluidic method, the PE multilayer covered bubbles may provide the constituents of highly stable gas capsules or foams which can be functionalised easily through the multilayer approach by adding a dedicated stratum in the millifluidic device [52,53]. Such functional capsules or foams may be interesting for medical applications or food design (using edible PEs). Translation of the method to droplets widens the range of applications, including, for example to cosmetics. One may also consider extraction and drying of the capsules provided the PE multilayer is sufficiently resistant.

CRediT authorship contribution statement

S. Pivard: Writing – review & editing, Writing – original draft, Visualization, Validation, Methodology, Investigation, Formal analysis, Data curation, Conceptualization. **A. Hourlier-Fargette:** Writing – review & editing, Methodology, Investigation, Conceptualization. **G. Cotte-Carluer:** Investigation, Data curation. **D. Chen:** Data curation. **A. Egele:** Investigation, Data curation. **C. Lambour:** Resources. **F. Schosseler:** Writing – review & editing, Writing – original draft, Validation, Supervision, Methodology, Investigation, Funding acquisition, Formal analysis, Data curation, Conceptualization. **W. Drenckhan-Andreatta:** Writing – review & editing, Writing – original draft, Validation, Supervision, Resources, Project administration, Methodology, Investigation, Funding acquisition, Formal analysis, Conceptualization.

Declaration of competing interest

The authors declare that they have no known competing financial interests or personal relationships that could have appeared to influence the work reported in this paper.

Data availability

Data will be made available on request.

Acknowledgements

The authors acknowledge fruitful discussions with Fouzia Boulmedais, Leandro Jacomine, Corentin Tregouët, Cécile Monteux, Olivier Felix and Michel Tschopp. S. P., A. H.-F., F. S. and W. D. acknowledge a brainstorming meeting with Jonathan Dijoux, Robin Bollache and Sébastien Andrieux, where the main idea of this project was born collectively. One of the reviewers is warmly acknowledged for a thorough reading that pointed out an error in our initial version of Eqs. (17)–(20). We thank the CARMAC facility from Institut Charles Sadron for characterisation of the polymer samples. This work has been financed by an ERC Consolidator Grant (agreement 819511 METAFOAM). It was conducted in the framework of the Interdisciplinary Institute HiFunMat, as part of the ITI 2021–2028 program of the University of Strasbourg, CNRS and Inserm, was supported by IdEx Unistra (ANR-10-IDEX-0002) and SFRI (STRATUS project, ANR-20-SFRI-0012) under the framework of the French Investments for the Future Program.

Appendix A. Supplementary data

Supplementary material related to this article can be found online at https://doi.org/10.1016/j.colsurfa.2024.134608.

References

[1] D. Guzey, D.J. McClements, Formation, stability and properties of multilayer emulsions for application in the food industry, Adv. Colloid Interf. Sci. 128–130 (2006) (2006) 227–248, http://dx.doi.org/10.1016/j.cis.2006.11.021.

[2] B.G. De Geest, S. De Koker, G.B. Sukhorukov, O. Kreft, W.J. Parak, A.G. Skirtach, J. Demeester, S.C. De Smedt, W.E. Hennink, Polyelectrolyte microcapsules for biomedical applications, Soft Matter 5 (2009) 282–291, http://dx.doi.org/10.1039/B808262F.

[3] E.M. Shchukina, D.G. Shchukin, Layer-by-layer coated emulsion microparticles as storage and delivery tool, Curr. Opin. Colloid Interf. Sci. 17 (5) (2012) 281–289, http://dx.doi.org/10.1016/j.cocis.2012.06.003.

[4] G. Bortnowska, Multilayer oil-in-water emulsions: Formation, characteristics and application as the carriers for lipophilic bioactive food components - A review, Polish J. Food Nutrit. Sci. 65 (3) (2015) 157–166, http://dx.doi.org/10.2478/v10222-012-0094-0.

[5] C. Burgos-Díaz, T. Wandersleben, A.M. Marqués, M. Rubilar, Multilayer emulsions stabilized by vegetable proteins and polysaccharides, Curr. Opin. Colloid Interf. Sci. 25 (2016) 51–57, http://dx.doi.org/10.1016/j.cocis.2016.06.014.

[6] T. Fu, Y. Ma, Bubble formation and breakup dynamics in microfluidic devices: A review, Chem. Eng. Sci. 135 (2015) 343–372, http://dx.doi.org/10.1016/j.ces.2015.02.016.

[7] K. Wang, Y.C. Lu, J.H. Xu, J. Tan, G.S. Luo, Generation of micromonodispersed droplets and bubbles in the capillary embedded T-junction microfluidic devices, AIChE J. 57 (2011) 299–306, http://dx.doi.org/10.1002/aic.12263.

[8] E. Donath, G.B. Sukhorukov, F. Caruso, S.A. Davis, H. Möhwald, Novel hollow polymer shells by colloid-templated assembly of polyelectrolytes, Angew. Chem. Intern. Ed. 37 (16) (1998) 2201–2205.

[9] G.B. Sukhorukov, E. Donath, H. Lichtenfeld, E. Knippel, M. Knippel, A. Budde, H. Möhwald, Layer-by-layer self assembly of polyelectrolytes on colloidal particles, Colloids Surf. A 137 (1–3) (1998) 253–266, http://dx.doi.org/10.1016/S0927-7757(98)00213-1.

[10] C. Gao, E. Donath, S. Moya, V. Dudnik, H. Möhwald, Elasticity of hollow polyelectrolyte capsules prepared by the layer-by-layer technique, Eur. Phys. J. E 5 (1) (2001) 21–27, http://dx.doi.org/10.1007/s101890170083.

[11] G.B. Sukhorukov, A.A. Antipov, A. Voigt, E. Donath, H. Möhwald, pH-controlled macromolecule encapsulation in and release from polyelectrolyte multilayer nanocapsules, Macromol. Rapid Comm. 22 (1) (2001) 44–46.

[12] O.I. Vinogradova, D. Andrienko, V.V. Lulevich, S. Nordschild, G.B. Sukhorukov, Young's modulus of polyelectrolyte multilayers from microcapsule swelling, Macromolecules 37 (3) (2004) 1113–1117, http://dx.doi.org/10.1021/ma0350213.

[13] V.V. Lulevich, D. Andrienko, O.I. Vinogradova, Elasticity of polyelectrolyte multilayer microcapsules, J. Chem. Phys. 120 (8) (2004) 3822–3826, http://dx.doi.org/10.1063/1.1644104.

[14] D.G. Shchukin, K. Köhler, H. Möhwald, G.B. Sukhorukov, Gas-filled polyelectrolyte capsules, Angew. Chem. Int. Edn 44 (21) (2005) 3310–3314, http://dx.doi.org/10.1002/anie.200462889.

[15] M. Winterhalter, A.F. Sonnen, Stable air bubbles - Catch them if you can!, Angew. Chem. Int. Edn 45 (16) (2006) 2500–2502, http://dx.doi.org/10.1002/anie.200504526.

[16] D.O. Grigoriev, T. Bukreeva, H. Möhwald, D.G. Shchukin, New method for fabrication of loaded micro- and nanocontainers: Emulsion encapsulation by polyelectrolyte layer-by-layer deposition on the liquid core, Langmuir 24 (3) (2008) 999–1004, http://dx.doi.org/10.1021/la702873f.

[17] H. Daiguji, E. Matsuoka, S. Muto, Fabrication of hollow poly-allylamine hydrochloride/poly-sodium styrene sulfonate microcapsules from microbubble templates, Soft Matter 6 (9) (2010) 1892–1897, http://dx.doi.org/10.1039/c000071j.

[18] M. Ruano, A. Mateos-Maroto, F. Ortega, H. Ritacco, J.E. Rubio, E. Guzmán, R.G. Rubio, Fabrication of robust capsules by sequential assembly of polyelectrolytes onto charged liposomes, Langmuir 37 (20) (2021) 6189–6200, http://dx.doi.org/10.1021/acs.langmuir.1c00341.

[19] S. Madisetti, Z. Zheng, Z. Gong, S. Penmetsa, Y. Lvov, L. Que, Layer-by-layer nanoscale-coating of microparticles with a droplet microfluidic device, in: 2009 4th IEEE International Conference on Nano/Micro Engineered and Molecular Systems, 2009, pp. 445–448, http://dx.doi.org/10.1109/NEMS.2009.5068615.

[20] S. Matosevic, B.M. Paegel, Stepwise synthesis of giant unilamellar vesicles on a microfluidic assembly line, J. Amer. Chem. Soc. 133 (9) (2011) 2798–2800, http://dx.doi.org/10.1021/ja109137s.

[21] C. Trégouët, Polymer Multilayers at Liquid Interfaces: Assembly, Interfacial Rheology and Microfluidic Probing (Ph.D. thesis), Université Pierre et Marie Curie, 2016.

[22] C. Trégouët, T. Salez, C. Monteux, M. Reyssat, Microfluidic probing of the complex interfacial rheology of multilayer capsules, Soft Matter 15 (2019) 2782–2790, http://dx.doi.org/10.1039/C8SM02507J.

[23] S. Zhang, L. Yobas, D. Trau, A microfluidic device for continuousflow layer-by-layer encapsulation of droplets with polyelectrolytes, in: 12th Intern. Conf. on Miniatur. Syst. for Chem. and Life Sci. - the Proceedings of MicroTAS 2008 Conference, 2008, pp. 1402–1404.

[24] R.D. Sochol, S. Li, L.P. Lee, L. Lin, Continuous flow multi-stage microfluidic reactors via hydrodynamic microparticle railing, Lab On a Chip 12 (20) (2012) 4168–4177, http://dx.doi.org/10.1039/c2lc40610a.

[25] C. Kantak, S. Beyer, L. Yobas, T. Bansal, D. Trau, A 'microfluidic pinball' for on-chip generation of Layer-by-Layer polyelectrolyte microcapsules, Lab Chip 11 (6) (2011) 1030–1035, http://dx.doi.org/10.1039/c0lc00381f.

[26] Y. Yan, M. Björnmalm, F. Caruso, Assembly of layer-by-layer particles and their interactions with biological systems, Chem. Mater. 26 (1) (2014) 452–460, http://dx.doi.org/10.1021/cm402126n.

[27] S.S.H. Tsai, J.S. Wexler, J. Wan, H.A. Stone, Conformal coating of particles in microchannels by magnetic forcing, Appl. Phys. Lett. 99 (15) (2011) 153509, http://dx.doi.org/10.1063/1.3652772.

[28] M.D. Tarn, R.F. Fakhrullin, V.N. Paunov, N. Pamme, Microfluidic device for the rapid coating of magnetic cells with polyelectrolytes, Mater. Lett. 95 (2013) 182–185, http://dx.doi.org/10.1016/j.matlet.2012.12.084.

[29] M. Björnmalm, A. Roozmand, K.F. Noi, J. Guo, J. Cui, J.J. Richardson, F. Caruso, Flow-based assembly of layer-by-layer capsules through tangential flow filtration, Langmuir 31 (33) (2015) 9054–9060, http://dx.doi.org/10.1021/acs.langmuir.5b02099.

[30] T. Okubo, Surface tension of synthetic polyelectrolyte solutions at the air-water interface, J. Colloid Interf. Sci. 125 (2) (1988) 386–398, http://dx.doi.org/10.1016/0021-9797(88)90003-3.

[31] G. Caminati, G. Gabrielli, Polystyrene sulfonate adsorption at water—graphon and water—air interfaces, Colloids Surf. A 70 (1) (1993) 1–14, http://dx.doi.org/10.1016/0927-7757(93)80491-V.

[32] H. Yim, M. Kent, A. Matheson, R. Ivkov, S. Satija, J. Majewski, G.S. Smith, Adsorption of poly(styrenesulfonate) to the air surface of water by neutron reflectivity, Macromolecules 33 (16) (2000) 6126–6133, http://dx.doi.org/10.1021/ma000266q.

[33] O. Théodoly, R. Ober, C.E. Williams, Adsorption of hydrophobic polyelectrolytes at the air/water interface: Conformational effect and history dependence, Eur. Phys. J. E 5 (1) (2001) 51–58, http://dx.doi.org/10.1007/s101890170086.

[34] B.A. Noskov, S.N. Nuzhnov, G. Loglio, R. Miller, Dynamic surface properties of sodium poly(styrenesulfonate) solutions, Macromolecules 37 (7) (2004) 2519–2526, http://dx.doi.org/10.1021/ma030319e.

[35] S. Pivard, L. Jacomine, F.S. Kratz, C. Foussat, J.-P. Lamps, M. Legros, F. Boulmedais, J. Kierfeld, F. Schosseler, W. Drenckhan, Interfacial rheology of linearly growing polyelectrolyte multilayers at the water-air interface: from liquid to solid viscoelasticity, Soft Matter 20 (2024) 1347–1360, http://dx.doi.org/10.1039/D3SM01161E.

[36] H. Ai, Y.M. Lvov, D.K. Mills, M. Jennings, J.S. Alexander, S.A. Jones, Coating and selective deposition of nanofilm on silicone rubber for cell adhesion and growth, Cell Biochem. Biophys. 38 (2) (2003) 103–114, http://dx.doi.org/10.1385/CBB:38:2:103.

[37] C.A. Schneider, W.S. Rasband, K.W. Eliceiri, NIH Image to ImageJ: 25 years of image analysis, Nat. Methods 9 (7) (2012/07/01) 671–675, http://dx.doi.org/10.1038/nmeth.2089.

[38] J. Schindelin, I. Arganda-Carreras, E. Frise, V. Kaynig, M. Longair, T. Pietzsch, S. Preibisch, C. Rueden, S. Saalfeld, B. Schmid, J.-Y. Tinevez, D.J. White, V. Hartenstein, K. Eliceiri, P. Tomancak, A. Cardona, Fiji: an open-source platform for biological-image analysis, Nat. Methods 9 (7) (2012/07/01) 676–682, http://dx.doi.org/10.1038/nmeth.2019.

[39] G. Ginot, R. Höhler, S. Mariot, A. Kraynik, W. Drenckhan, Juggling bubbles in square capillaries: an experimental proof of non-pairwise bubble interactions, Soft Matter 15 (22) (2019) 4570–4582, http://dx.doi.org/10.1039/C8SM02477D.

[40] M. Belloul, W. Engl, A. Colin, P. Panizza, A. Ajdari, Competition between local collisions and collective hydrodynamic feedback controls traffic flows in microfluidic networks, Phys. Rev. Lett. 102 (2009) 194502, http://dx.doi.org/10.1103/PhysRevLett.102.194502.

[41] G.F. Christopher, S.L. Anna, Microfluidic methods for generating continuous droplet streams, J. Phys. D: Appl. Phys. 40 (19) (2007) R319, http://dx.doi.org/10.1088/0022-3727/40/19/R01.

[42] C.J. Martinez, Bubble generation in microfluidic devices , Bubble Sci. Engin. Techn. 1 (1–2) (2009) 40–52.

[43] P. Zhu, L. Wang, Passive and active droplet generation with microfluidics: a review, Lab Chip 17 (2016) 34–75, http://dx.doi.org/10.1039/C6LC01018K.

[44] M. Costantini, J. Jaroszewicz, L. Kozon, K. Szlazak, W. Swieszkowski, P. Garstecki, C. Stubenrauch, A. Barbetta, J. Guzowski, 3D printing of functionally graded porous materials using on-demand reconfigurable microfluidics, Angew. Chem. Int. Edn 58 (2019) 7620–7625, http://dx.doi.org/10.1002/anie.201900530.

[45] P. Garstecki, A.M. Ganan-Calvo, G.M. Whitesides, Formation of bubbles and droplets in microfluidic systems, Bull. Polish Acad. Sci. Tech. Sci. 53 (2005) 361.

[46] P. Garstecki, M.J. Fuerstman, H.A. Stone, G.M. Whitesides, Formation of droplets and bubbles in a microfluidic T-junction - Scaling and mechanism of break-up, Lab Chip 6 (3) (2006) 437–446, http://dx.doi.org/10.1039/b510841a.

[47] F. White, J. Madjalani, Viscous Fluid Flow, fourth ed., Mc Graw Hill, 2022.

[48] F.P. Bretherton, The motion of long bubbles in tubes, J. Fluid Mech. 10 (1961) 166.

[49] A. Saugey, W. Drenckhan, D. Weaire, Wall slip of bubbles in foams, Phys. Fluids 18 (5) (2006) 053101, http://dx.doi.org/10.1063/1.2196912.
[50] P. Sajeesh, M. Doble, A.K. Sen, Hydrodynamic resistance and mobility of deformable objects in microfluidic channels, Biomicrofluidics 8 (5) (2014) 054112, http://dx.doi.org/10.1063/1.4897332.
[51] W. Kloek, T. van Vliet, M. Meinders, Effect of bulk and interfacial rheological properties on bubble dissolution, J. Colloid Interf. Sci. 237 (2) (2001) 158–166, http://dx.doi.org/10.1006/jcis.2001.7454.
[52] L. Seón, P. Lavalle, P. Schaaf, F. Boulmedais, Polyelectrolyte multilayers: A versatile tool for preparing antimicrobial coatings, Langmuir 31 (2015) 12856–12872, http://dx.doi.org/10.1021/acs.langmuir.5b02768.
[53] C. Vigier-Carrière, T. Garnier, D. Wagner, P. Lavalle, M. Rabineau, J. Hemmerlé, B. Senger, P. Schaaf, F. Boulmedais, L. Jierry, Bioactive seed layer for surface-confined self-assembly of peptides, Angew. Chem. Int. Edn 54 (35) (2015) 10198–10201, http://dx.doi.org/10.1002/anie.201504761.